

Ferroelectric-Gated InSe Photodetectors with High On/Off Ratios and Photoresponsivity

Li Liu, Liangmei Wu, Aiwei Wang, Hongtao Liu, Ruisong Ma, Kang Wu, Jiancui Chen, Zhang Zhou, Yuan Tian, Haitao Yang, Chengmin Shen, Lihong Bao,* Zhihui Qin,* Sokrates T. Pantelides, and Hong-Jun Gao

Cite This: *Nano Lett.* 2020, 20, 6666–6673

Read Online

ACCESS |

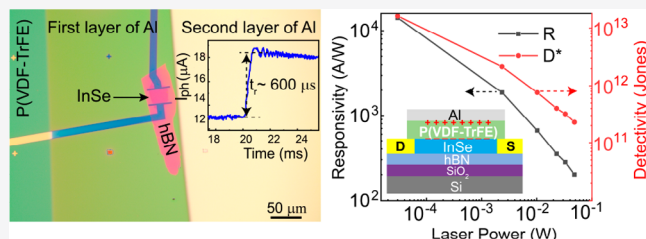
Metrics & More

Article Recommendations

Supporting Information

ABSTRACT: Indium selenide (InSe) has a high electron mobility and tunable direct band gap, enabling its potential applications to electronic and optoelectronic devices. Here, we report the fabrication of InSe photodetectors with high on/off ratios and ultrahigh photoresponsivity, using ferroelectric poly(vinylidene fluoride-trifluoroethylene) (P(VDF-TrFE)) copolymer films as the top-gate dielectric. Benefiting from the successful suppression of the dark current down to $\sim 10^{-14}$ A in the InSe channel by tuning the three different polarization states in ferroelectric P(VDF-TrFE) and improved interface properties using h-BN as a substrate, the ferroelectric-gated InSe photodetectors show a high on/off ratio of over 10^8 , a high photoresponsivity up to $14\,250\text{ AW}^{-1}$, a high detectivity up to 1.63×10^{13} Jones, and a fast response time of $600\ \mu\text{s}$ even at zero-gate voltage. The present results highlight the role of ferroelectric P(VDF-TrFE) in tuning the carrier transport of InSe and may provide an avenue for the development of InSe-based photodetectors.

KEYWORDS: InSe, P(VDF-TrFE), ferroelectric, photodetector, on/off ratios, photoresponsivity



Ultrathin films of layered materials have captured considerable attention because of their fascinating physical properties that vary with reduced thickness, which in recent years have been shown to be promising for a bewildering variety of applications to photonic and optoelectronic devices.^{1,2} Photodetectors, as a key component of optoelectronic applications, have attracted widespread interest,^{3–6} and, in recent years, a major focus has been on phototransistors based on two-dimensional (2D) materials.^{7–9} Except for semimetallic graphene,^{10,11} many semiconducting 2D materials have emerged as possible channel materials for photodetectors. Among them, the family of transition-metal dichalcogenides (TMDs),^{12–15} silicene,¹⁶ and black phosphorus (BP)¹⁷ overcome the shortcomings of the zero band gap of graphene. However, an intrinsic bottleneck of these 2D materials is the small photoswitch ratio and photoresponsivity due to the large dark current under the needed large gate voltages.

Indium selenide (InSe), a representative example of a 2D III–VI semiconductor, shows fascinating electrical transport properties with charge carrier mobility of $\sim 10^4\text{ cm}^2\text{ V}^{-1}\text{ s}^{-1}$ and broad spectral response bandwidth covering the waves from ultraviolet to near-infrared because of its moderate and tunable direct band gap,^{18,19} enabling it as an attractive building block for optoelectronic devices.^{20–22} Field-effect transistors (FETs) based on InSe and conventional dielectrics, such as Al_2O_3 ,²³ SiO_2 ,^{24–27} and HfO_2 ,^{28,29} as back-gate

dielectrics, have an on/off ratio as high as 4.7×10^4 (ref 27), responsivity as high as 157 AW^{-1} (ref 25), and detectivity up to 1.07×10^{11} (ref 25), but require large V_g (20–100 V) and V_{DS} (1–10 V) voltage bias (see Table 1). Furthermore, a sizable dark current is generated by large voltages used in back-gate configurations, increasing the risk of leakages.^{30–32} Compared to conventional dielectrics, ferroelectric dielectrics have the advantages of high dielectric constants ($\epsilon_r \sim 10^3$).³³ InAs-based mid-infrared photodetectors with the organic ferroelectric P(VDF-TrFE) dielectric layers possess 3–4 orders of magnitude higher photoresponsivity than commercially available devices, benefiting from suppression of dark current and enhancement of photoresponsivity by the ferroelectric films.³⁴ Also, greatly enhanced performance in MoS_2 and MoTe_2 photodetectors has been achieved by employing P(VDF-TrFE) as a gate insulator,^{35–38} benefiting from its transparent nature, high ambient stability, and effective passivation or encapsulation of 2D material surfaces by hydrogen or fluorine atoms. However, whether the P(VDF-

Received: June 16, 2020
 Revised: August 20, 2020
 Published: August 21, 2020

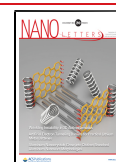
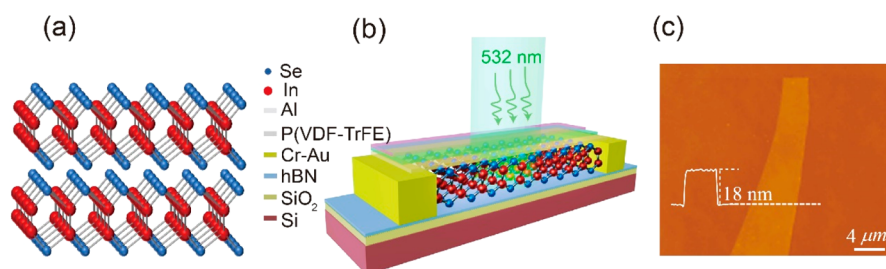


Table 1. Comparison of the Performance of Our Device with Other InSe-Based Devices and Ferroelectric-Gated Photodetectors

photodetector		wavelength/power density	on/off	response time (ms)	recovery time (ms)	R (mAW ⁻¹)	D* (Jones)	ref
traditionally gated InSe devices	InSe	532 nm 2.5 mW/mm ²		488 μs		34.7		24
	InSe-SiO ₂ -Si	633 nm 2.1 mW/cm ²		50		157 000	1.07 × 10 ¹¹	25
	InSe-SiO ₂ -Si	635 nm 0.2 W/cm ²	10 ⁴			590		27
similar ferroelectric-gated devices	P(VDF-TrFE)-MoS ₂	635 nm 1 nW	~10 ⁵	1.8	2.0	2 570 000	2.2 × 10 ¹²	35
	P(VDF-TrFE)-MoTe ₂	1060 nm 10 μW	~10 ⁴	1.4	1.3	16.4	1.94 × 10 ⁸	36
	P(VDF-TrFE)-MoS ₂	10 μm 130 nW	10 ³	5.5		140		37
	P(VDF-TrFE)-InP	830 nm 0.07 mW/cm ²	~10 ⁵	29.1	139.6	280 000 000	9.1 × 10 ¹⁵	46
P(VDF-TrFE)-InSe	532 nm 0.04 mW/cm ²	~10 ⁸	600 μs	1.2	14 250 000	1.63 × 10 ¹³	this work	

**Figure 1.** Components of a multilayered InSe photodetector. (a) The crystal structure of γ -InSe. (b) Schematic device structure of a multilayered InSe photodetector under monochromatic light beam illumination. Multilayered InSe flake, h-BN on SiO₂/Si, Cr/Au metal stacks, P(VDF-TrFE), and Al are used as the channel material, substrate, contact electrodes, top-gate dielectric, and top-gate electrode, respectively. (c) Atomic force microscopy image of a selected 18 nm thick InSe flake.

TrFE) film as a top-gate dielectric can enhance photodetection performance in InSe photodetectors remains elusive.

Here we report the fabrication of ferroelectrically gated InSe photodetectors employing the P(VDF-TrFE) copolymer as the top gate, exhibiting high on/off ratios and ultrahigh photoresponsivity. Through tuning the three different polarization states in ferroelectric P(VDF-TrFE) copolymer films, the dark current in the InSe photodetectors is successfully suppressed down to $\sim 10^{-14}$ A. At the same time, hexagonal boron nitride (h-BN) is used as a substrate to improve the interface between the insulating substrate and the InSe channel. As a result, the ferroelectric copolymer-gated InSe photodetectors not only show a high on/off ratio of over 10^8 but also exhibit high photoresponsivity up to $14\,250\text{ AW}^{-1}$ and detectivity up to 1.63×10^{13} Jones even without gate voltage in the polarization-up state. Moreover, the measured rise (t_r) and fall (t_f) time of the photocurrent are $600\ \mu\text{s}$ and $1.2\ \text{ms}$, respectively. The present results provide an unprecedented avenue for developing high-performing InSe-based phototransistors.

Figure 1a schematically shows the crystal structure of monolayer InSe, which is composed of In–Se–Se–In layers forming a honeycomb lattice in the top view, stacked by van der Waals interactions.^{39,40} A stereogram of the device structure of the multilayered InSe photodetector under laser-beam illumination is depicted in Figure 1b. First, a mechanically exfoliated hBN flake ($\sim 10\ \text{nm}$) was stacked onto a p++-doped silicon substrate covered with a silicon

dioxide film of $300\ \text{nm}$. Then, a multilayered γ -InSe flake, stacked onto the h-BN layer by a dry-transfer method, was used as the semiconducting channel. A standard e-beam lithography technique was employed to define the contact electrodes followed by e-beam evaporation of a $6\ \text{nm Cr}/60\ \text{nm Au}$ metal stack. After lift-off, the InSe FETs were covered with a layer of about $300\ \text{nm}$ P(VDF-TrFE) film as the ferroelectric dielectric, which possesses a remanent polarization of $7\ \mu\text{C cm}^{-2}$ and coercive voltage of $22.5\ \text{V}$.^{35,41} To avoid the thickness and the transparency of the top-gate aluminum affecting the photoresponse performance of the InSe photodetectors, the first layer of $15\ \text{nm}$ thick aluminum near the channel region was deposited by e-beam evaporation as a semitransparent optical window to allow light illumination on the channel, and the second layer of $50\ \text{nm}$ thick aluminum far away from the channel region was deposited as the top-gate electrode, as demonstrated in Figure S1 (see Methods for details and Figure S1). An atomic force microscopy image of a selected $\sim 18\ \text{nm}$ thick InSe flake used as the channel material is shown in Figure 1c.

Electrical characterization of the ferroelectric-gated InSe FET was performed under darkness at room temperature. The transfer curves of the device are shown in linear scales in Figure 2a and logarithmic scales in Figure 2b, respectively. From Figure 2a, the carrier mobility in the InSe channel is extracted as $\mu = 272.9\ \text{cm}^2\ \text{V}^{-1}\ \text{s}^{-1}$ from $\mu = (L/W(1/(\epsilon_0\epsilon_r/d) \times V_{\text{DS}})(dI_{\text{DS}}/dV_{\text{tg}}))$,⁴² where L represents the channel length of

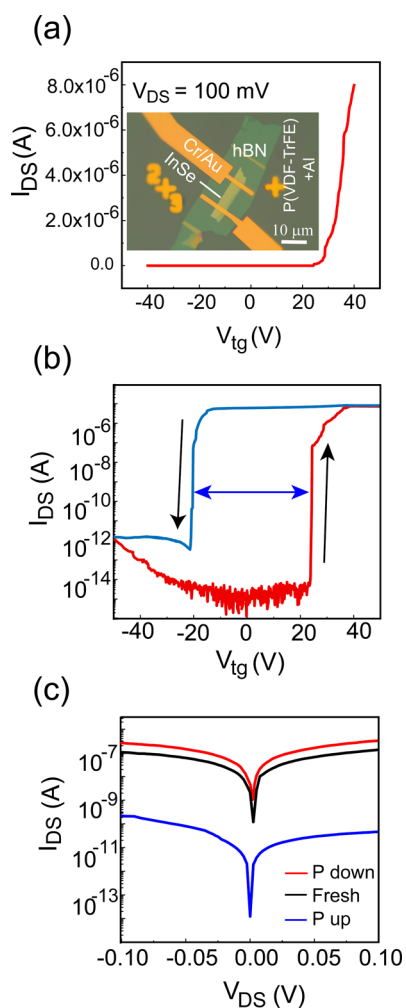


Figure 2. Electrical characterization of the ferroelectrically gated InSe transistor under darkness at room temperature. (a) Transfer curves of the InSe transistor using P(VDF-TrFE) as a ferroelectric top-gate dielectric at $V_{DS} = 100$ mV in linear (the inset presents an optical image of the transistor) and logarithmic scales in panel b. A large anticlockwise memory window of ~ 40 V is observed from dually sweeping from -40 to 40 V. (c) The output characteristics of the InSe FET with three states of ferroelectric film under zero-gate voltage. A pulse of ± 40 V is applied to achieve the down/up state of polarization of P(VDF-TrFE) (P down/up), and no pulse is applied for the fresh state without polarization.

$21 \mu\text{m}$, W represents the channel width of $5.2 \mu\text{m}$, ϵ_0 represents the vacuum dielectric of $8.854 \times 10^{-12} \text{Fm}^{-1}$, ϵ_r represents the relative dielectric constant of P(VDF-TrFE) of 10, d represents the 300 nm thick ferroelectric film, and $V_{DS} = 100$ mV represents the drain–source voltage, respectively. As demonstrated in Figure 2b, the transfer curves of the multilayer InSe channel under ferroelectric P(VDF-TrFE) modulation when sweeping the gate voltage from -40 to 40 V and back at $V_{DS} = 100$ mV, show a large anticlockwise memory window of ~ 40 V, which results from the ferroelectric-polarization switching process. Moreover, under a 100 mV drain–source voltage, the channel current (I_{DS}) increases with increasing top-gate voltage (V_{tg}), indicating a typical n-type conduction in the InSe channel, which is in line with previous reports.^{43,44} The current on/off ratio reaches as high as $\sim 10^8$, which is attributed to the better interface quality between InSe and hBN.⁴⁴ As shown in Figures S2–S4, with the selected hBN

sandwiched between the InSe and SiO_2 layers, the current on/off ratio of the P(VDF-TrFE)/InSe/hBN device (Figure S2) in the dark state at room temperature is significantly improved from 10^5 of P(VDF-TrFE)/InSe/ SiO_2 (Figure S2b) to 10^8 (Figure S3b and Figure S4b).

Figure 3a–c schematically demonstrates the three different polarization states of ferroelectric P(VDF-TrFE) films: polarization-down state, fresh state (without polarization), and polarization-up state,⁴⁵ respectively. The polarization-down (-up) state can be obtained by employing a 40 V (-40 V) pulse voltage with a pulse width of 3 s to the P(VDF-TrFE) film. The output characteristics of InSe FET under the modulation of the three states of the ferroelectric P(VDF-TrFE) film are exhibited in Figure 2c. It is found that the channel current I_{DS} in the polarization-up state is the smallest among these three states. The reason is that carriers in the InSe channel are completely depleted in the polarization-up state, which arises from the poling field generated by the remanent polarization of ferroelectric P(VDF-TrFE) thin film.³⁵ More specifically, the dark current of the InSe channel is successfully suppressed down to $\sim 10^{-14}$ A by the ferroelectric P(VDF-TrFE) copolymer film in the polarization-up state. We also find that the remanent polarization field of the top-gate dielectric can successfully suppress the dark current of thicker InSe (~ 36 nm), as shown in Figure S4c. On the contrary, the carriers are accumulated in the polarization-down state, resulting in a high channel current.

One of the key figures of merit in photodetectors is the photoresponsivity. The dependence of the photoresponsivity of the ferroelectric-gated InSe photodetector on the different ferroelectric polarization states and various laser power intensities at zero-gate voltage is demonstrated in Figure 3. The different polarization state in the ferroelectric film is presupposed to a specific polarization state (polarization-up or polarization-down) by applying a short bias pulse to the P(VDF-TrFE) film before the photoresponsivity measurement. Under illumination by a 532 nm laser, different power levels of 0.1%, 10%, 32%, 50%, 79%, and 100% correspond to illumination intensities of 0.04, 2.98, 12.99, 29.17, 41.91, and 61.40 mW/cm^2 , respectively. The I_{DS} – V_{DS} curves of the photodetector with the three polarization states under darkness and varying illuminating laser powers at a 532 nm wavelength are demonstrated in Figure 3d–f, all of them are symmetric and linear. Comparing the results of the three polarization states, it is obvious that, at $V_{DS} = 0.1$ V, under full light illumination, I_{DS} in the polarization-up state, fresh state, and polarization-down state are 12, 23, and ~ 700 nA, respectively. That means, I_{DS} is the smallest in the polarization-up state, which is in accordance with the above results (Figure 2c). For the polarization-up state, the dark current is also the smallest, suggesting that the remanent poling field of the ferroelectric P(VDF-TrFE) film can effectively suppress the dark current of the InSe semiconducting channel.³⁴ In other words, the dark current is restrained in the polarization-up state and enhanced in the polarization-down state. In an ultrahigh poling field generated by the ferroelectric top-gate dielectric,⁴⁶ the InSe channel is kept in the completely depleted state, whereby the sensitivity of the phototransistor can be prominently improved even at zero-gate voltage. The photoswitching behaviors in the corresponding ferroelectric polarization state under a wavelength of 532 nm and $V_{DS} = 0.1$ V are depicted in Figure 3g–i. I_{ph} of the polarization-up state is the smallest among the different three states. The channel current in the fresh state

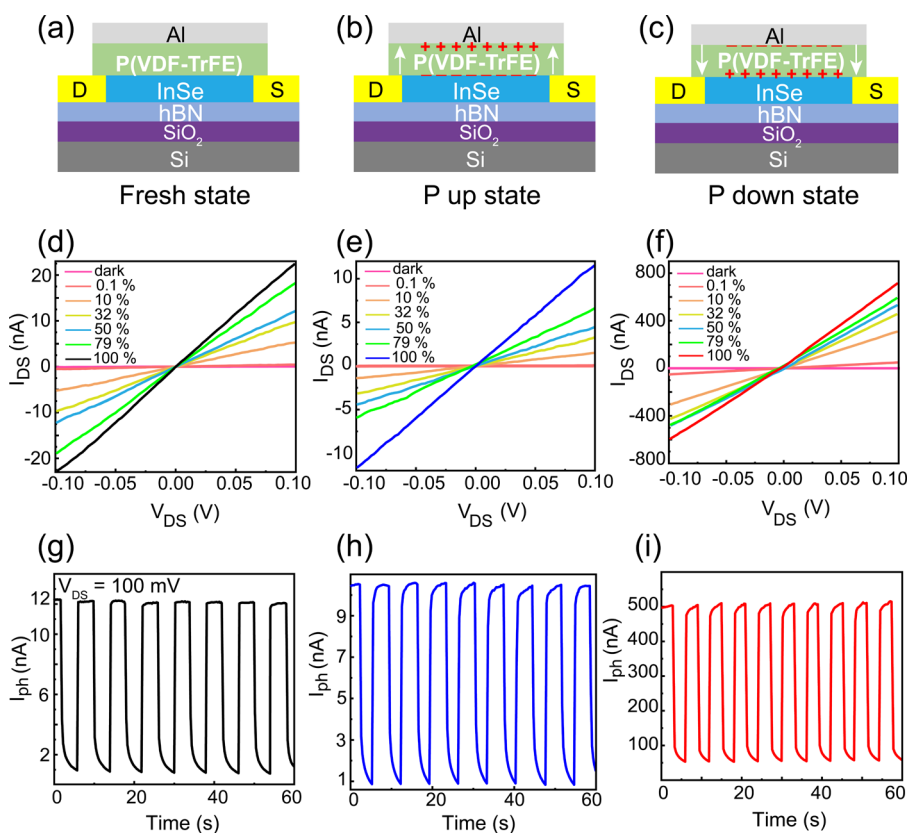


Figure 3. Photoresponse characteristics of the multilayered InSe phototransistor under the three polarization states of the ferroelectric P(VDF-TrFE) layer at zero-gate voltage. (a–c) The cross-sectional diagrams of the InSe phototransistor with the three different ferroelectric polarization states under $V_{DS} = 0$ V. (d–f) I_{DS} – V_{DS} characteristics of the phototransistor under darkness and illumination with varying power levels (the incident light wavelength is 532 nm, and a rated power level is 80 mW) at the three states illustrated in panels a–c. The power density of 0.1%–100% P is quantified as 0.04, 2.98, 12.99, 29.17, 41.91, and 61.40 mW/cm^2 , respectively. (g–i) The photoswitching properties of the ferroelectric gated InSe photodetector at the three states illustrated in panels a–c ($\lambda = 532$ nm, $V_{DS} = 100$ mV, $P = 61.40$ mW/cm^2).

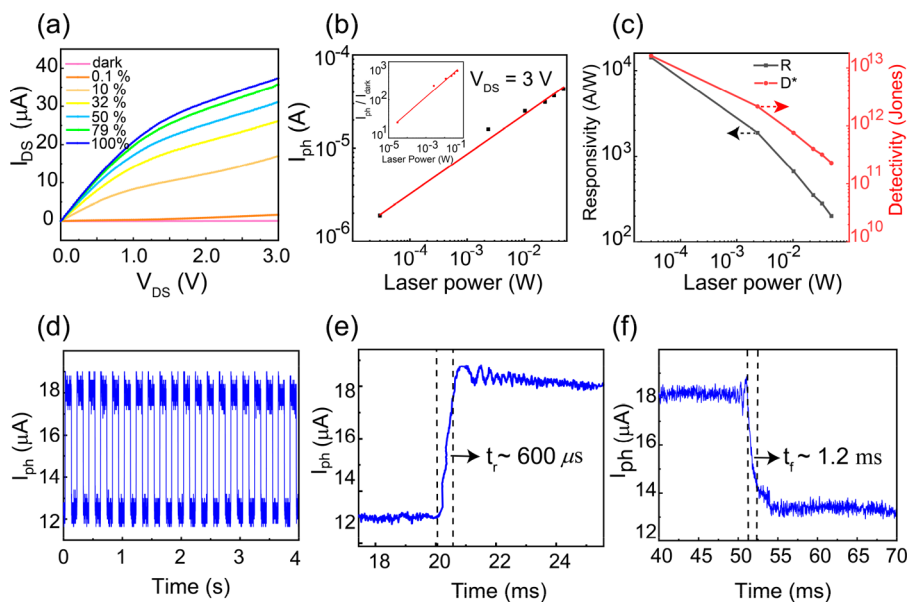


Figure 4. Photoresponse characteristics of a ferroelectric-gated InSe photodetector in the polarization-up state ($\lambda = 532$ nm, $V_{DS} = 3$ V). (a) I_{DS} – V_{DS} behaviors of the phototransistor under darkness and varying illuminating laser powers. (b) Illumination-power-dependent photocurrent. The inset is the relationship of I_{ph}/I_{dark} with different laser powers. (c) Responsivity and detectivity of the InSe photodetector, showing high responsivity of 14 250 AW^{-1} and high detectivity of 1.63×10^{13} Jones under the laser power of 0.04 mW/cm^2 . (d–f) Time-resolved photoswitching behavior of the InSe phototransistor in the polarization-up state ($\lambda = 532$ nm, $V_{DS} = 3$ V, $P = 61.40$ mW/cm^2).

and the polarization-down state is provided by both photo-excited carriers and thermionic/tunneling carriers. On the other hand, the channel current in the polarization-up state is dominated by the photogenerated current, which leads to efficient photocurrent extraction and enhanced photoresponse.⁴⁷

To further improve the optoelectric response characteristics, we characterize the photoresponse features of the ferroelectrically gated multilayered InSe phototransistor in the polarization-up state with $V_{DS} = 3$ V. Figure 4a exhibits the drain-source behaviors of the photodetector under darkness and varying illuminating laser powers. With the enhancement of the illuminating intensity, the channel current increases significantly from 72 nA in the dark state to 37 μ A under full laser illumination. This increase means that the photogenerated carriers contribute dominantly to the total current of the InSe semiconducting channel. In order to intuitively reveal the relationship between the photocurrent I_{ph} ($I_{ph} = I_{light} - I_{dark}$) and the laser power, the illumination power-dependent photocurrent is measured at $V_{DS} = 3$ V, which reveals that the photocurrent is power-law dependent on the illumination power: $I_{ph} \approx P^{0.44}$, as depicted in Figure 4b. It indicates that the efficiency of photogenerated carriers is not linearly dependent on the absorbed photon flux. The power-law relationship between photocurrent and the illumination power reflects the loss of the photogenerated carriers by a recombination process (the trap states),^{25,35,36,48} in which the defects of the InSe, the charge impurities around the InSe, and the adsorbed molecules could be recombination centers. As the laser intensity increases, photogenerated carriers occupy more traps, resulting in the final saturation of the photocurrent. The relationship of I_{ph}/I_{dark} with different laser powers is shown in the inset of Figure 4b, implying that the present devices are very sensitive to the laser power. As is known, R (responsivity) and D^* (detectivity) are two key figures of merit characterizing the performance of phototransistors.⁴⁶ R can be extracted from the formula $R = I_{ph}/P \times S$, where P represents laser power density, S represents the effective channel excitation area, and $D^* = RS^{1/2}/(2eI_{dark})$.^{49,50} The extracted power-dependent responsivity and detectivity are depicted in Figure 4c. The phototransistor exhibits high photoresponsivity up to 14 250 AW^{-1} and high detectivity up to 1.63×10^{13} Jones (under low laser power 0.04 mW/cm^2), which are 2 orders of magnitude larger than the previously reported results of $R = 157$ AW^{-1} and $D^* \sim 10^{11}$ Jones (2.1 mW/cm^2 , $V_{DS} = 10$ V, and $V_{bg} = 70$ V), respectively.²⁵ As the laser power boosts, the high responsivity rate and detectivity decrease sharply, largely because of some recombination processes at the interface between InSe and the top-gate P(VDF-TrFE) layer. Time-resolved photoswitching behavior of the InSe photodetector in the polarization-up state under a wavelength of 532 nm with $V_{DS} = 3$ V are demonstrated in Figure 4d. The rise (t_r) and fall (t_f) time are measured as 600 μ s and 1.2 ms, respectively, which is faster than the currently reported ferroelectric-gated 2D photodetectors.^{35–37,46} Compared with Figure 3i, the I_{ph} is greatly improved from the order of \sim nA to \sim μ A due to the increase of the drain-source voltage. When $V_{DS} = 100$ mV, the maximum photoresponsivity value is just 420 AW^{-1} (Figure S4b), which is two orders lower than the case of $V_{DS} = 3$ V. This phenomenon can be explained by the light absorption and excitation of electron-hole pairs under laser illumination.⁴⁶

For the sake of illustrating the outstanding performance of ferroelectric-gated InSe phototransistors more intuitively, comparison of key figures of merit between traditionally gated InSe photodetectors and similar ferroelectric-gated photodetectors are shown in Table 1. The on/off ratio, R , and D^* of the present ferroelectric-gated InSe photodetector are obviously superior to those of other traditionally gated InSe phototransistors.^{24,25,27} Compared with similar ferroelectric-gated devices, the present InSe-based devices have a higher on/off ratio by at least 3 orders of magnitude and the shortest response and recovery times.^{35–37} They also have comparably very high R and D^* values, but InP-based devices exceed the present values.⁴⁶ The reasons for such excellent performance can be summarized into the following three points: (1) The dielectric constant of the top-gate dielectric is about 10 times larger than that of SiO_2 and Al_2O_3 ,^{23,24} which results in better dielectric screening performance.⁴⁵ (2) Compared to the previous back-gate FETs,⁵¹ InSe is sandwiched between the hBN and P(VDF-TrFE) film, which can prevent its degradation and additional scattering from water, oxygen, and adsorbed molecules in the air.²⁷ Furthermore, the high-quality interface between InSe and hBN greatly suppresses charge impurity scattering from the SiO_2 substrate.⁴⁴ (3) The remnant polarization field of the polarization-up state can fully deplete the concentration of carriers caused by defect/trap states;⁴⁶ therefore, the dark current of our device was successfully suppressed down to 10^{-14} A.

In conclusion, we have successfully fabricated ferroelectrically gated InSe photodetectors with high current on/off ratios ($\sim 10^8$) and ultrahigh photoresponsivity (~ 14 250 AW^{-1}) because of the effective suppression of the dark current by depleting carriers in the InSe channel at the polarization-up state of the ferroelectric P(VDF-TrFE) top-gate dielectric. The InSe phototransistor under ferroelectric layer modulation even at zero-gate voltage manifests remarkable photodetection performance compared to those using traditional dielectrics. The transparent nature, high ambient stability, and effective passivation or encapsulation of recombination centers on 2D material surfaces by hydrogen or fluorine atoms of ferroelectric P(VDF-TrFE) films greatly enhance photodetection performance in InSe photodetectors and will be promising in the development of future 2D high-performance photodetectors.

Methods. Sample Preparation. The InSe and hBN nanosheets were obtained by mechanical exfoliation of the commercial γ -InSe bulk crystal (2D Semiconductors) and BN single crystal (HQ Graphene), respectively. Then InSe/hBN heterostructures were prepared by the dry-transfer technique.^{52,53} All of the exfoliation and stacking processes were carried out in a glovebox filled with highly purified Ar.

Measurement of InSe Thickness. Atomic force microscopy (AFM, Asylum Research, Cypher S) experiments were performed under ambient conditions with the tapping mode to measure the thicknesses of InSe and hBN flakes.

Device Fabrication. For the sake of avoiding degradation of the InSe/hBN heterostructures, the sample was spin-coated with poly(methyl methacrylate) (PMMA) in a glovebox before device fabrication. Electron beam lithography (Raith 150) was used to pattern the contact electrodes. Six nm Cr followed by 60 nm Au were deposited by electron beam evaporation used as metal contacts. After lift-off, the InSe FETs were covered with the 2.5 wt % P(VDF-TrFE) solution by spin-casting in the glovebox. The P(VDF-TrFE) films were baked at 135 $^{\circ}C$ in a vacuum oven for 2 h to increase the crystallinity. At last, the

first layer of 15 nm thick aluminum near the channel region was deposited by e-beam evaporation as a semitransparent optical window to allow light illumination on the channel, and the second layer of 50 nm thick aluminum far away from the channel region was deposited as the top-gate electrode patterned by a “shadow mask”.

Device Performance Measurement. The measurements of electronic and optoelectronic performance of fabricated devices were measured under a vacuum at room temperature, employing a Keithley 4200 semiconductor characterization system and a Lakeshore probe station. The InSe photo-transistors were illuminated at a 532 nm wavelength, and the intensity of the incident laser source was measured by an optical power meter. To achieve different powers of illumination, an attenuator was used.

■ ASSOCIATED CONTENT

SI Supporting Information

The Supporting Information is available free of charge at <https://pubs.acs.org/doi/10.1021/acs.nanolett.0c02448>.

Additional figures regarding optical images of devices; electrical and photoresponse characterization of additional devices with different thicknesses of InSe flakes (PDF)

■ AUTHOR INFORMATION

Corresponding Authors

Lihong Bao – Institute of Physics & University of Chinese Academy of Sciences, Chinese Academy of Sciences, Beijing 100190, People’s Republic of China; Songshan Lake Materials Laboratory, Dongguan, Guangdong 523808, People’s Republic of China; orcid.org/0000-0002-2942-892X; Email: lhbao@iphy.ac.cn

Zhihui Qin – Key Laboratory for Micro/Nano Optoelectronic Devices of Ministry of Education & Hunan Provincial Key Laboratory of Low-Dimensional Structural Physics and Devices, School of Physics and Electronics, Hunan University, Changsha 410082, People’s Republic of China; Email: zhqin@hnu.edu.cn

Authors

Li Liu – Key Laboratory for Micro/Nano Optoelectronic Devices of Ministry of Education & Hunan Provincial Key Laboratory of Low-Dimensional Structural Physics and Devices, School of Physics and Electronics, Hunan University, Changsha 410082, People’s Republic of China; Institute of Physics & University of Chinese Academy of Sciences, Chinese Academy of Sciences, Beijing 100190, People’s Republic of China

Liangmei Wu – Institute of Physics & University of Chinese Academy of Sciences, Chinese Academy of Sciences, Beijing 100190, People’s Republic of China

Aiwei Wang – Institute of Physics & University of Chinese Academy of Sciences, Chinese Academy of Sciences, Beijing 100190, People’s Republic of China

Hongtao Liu – Institute of Physics & University of Chinese Academy of Sciences, Chinese Academy of Sciences, Beijing 100190, People’s Republic of China

Ruisong Ma – Institute of Physics & University of Chinese Academy of Sciences, Chinese Academy of Sciences, Beijing 100190, People’s Republic of China

Kang Wu – Institute of Physics & University of Chinese Academy of Sciences, Chinese Academy of Sciences, Beijing 100190, People’s Republic of China

Jiancui Chen – Institute of Physics & University of Chinese Academy of Sciences, Chinese Academy of Sciences, Beijing 100190, People’s Republic of China

Zhang Zhou – Institute of Physics & University of Chinese Academy of Sciences, Chinese Academy of Sciences, Beijing 100190, People’s Republic of China

Yuan Tian – Key Laboratory for Micro/Nano Optoelectronic Devices of Ministry of Education & Hunan Provincial Key Laboratory of Low-Dimensional Structural Physics and Devices, School of Physics and Electronics, Hunan University, Changsha 410082, People’s Republic of China

Haitao Yang – Institute of Physics & University of Chinese Academy of Sciences, Chinese Academy of Sciences, Beijing 100190, People’s Republic of China

Chengmin Shen – Institute of Physics & University of Chinese Academy of Sciences, Chinese Academy of Sciences, Beijing 100190, People’s Republic of China; Songshan Lake Materials Laboratory, Dongguan, Guangdong 523808, People’s Republic of China

Sokrates T. Pantelides – Department of Physics and Astronomy and Department of Electrical Engineering and Computer Science, Vanderbilt University, Nashville, Tennessee 37235, United States; Institute of Physics & University of Chinese Academy of Sciences, Chinese Academy of Sciences, Beijing 100190, People’s Republic of China; orcid.org/0000-0002-2963-7545

Hong-Jun Gao – Institute of Physics & University of Chinese Academy of Sciences, Chinese Academy of Sciences, Beijing 100190, People’s Republic of China; Songshan Lake Materials Laboratory, Dongguan, Guangdong 523808, People’s Republic of China; orcid.org/0000-0002-6766-0623

Complete contact information is available at: <https://pubs.acs.org/doi/10.1021/acs.nanolett.0c02448>

Notes

The authors declare no competing financial interest.

■ ACKNOWLEDGMENTS

This work was supported by the National Key Research & Development Projects of China (2016YFA0202300 and 2018FYA0305800), National Natural Science Foundation of China (61674170, 51772087, and 61888102), Strategic Priority Research Program of Chinese Academy of Sciences (CAS, XDB30000000 and XDB28000000), and Youth Innovation Promotion Association of CAS (Y201902). The financial support from the Hunan Provincial Innovation Foundation for Postgraduates (CX2018B225). Work at Vanderbilt is partially supported by the McMinn Endowment. The authors gratefully acknowledge Haifang Yang, Junjie Li, and Changzhi Gu for help in device fabrication.

■ REFERENCES

- (1) Bonaccorso, F.; Sun, Z.; Hasan, T.; Ferrari, A. C. Graphene Photonics and Optoelectronics. *Nat. Photonics* **2010**, *4* (9), 611–622.
- (2) Lopez-Sanchez, O.; Lembke, D.; Kayci, M.; Radenovic, A.; Kis, A. Ultrasensitive Photodetectors Based on Monolayer MoS₂. *Nat. Nanotechnol.* **2013**, *8* (7), 497–501.
- (3) Buscema, M.; Groenendijk, D. J.; Blanter, S. I.; Steele, G. A.; van der Zant, H. S. J.; Castellanos-Gomez, A. Fast and Broadband

Photoresponse of Few-Layer Black Phosphorus Field-Effect Transistors. *Nano Lett.* **2014**, *14* (6), 3347–3352.

(4) Roy, K.; Padmanabhan, M.; Goswami, S.; Sai, T. P.; Ramalingam, G.; Raghavan, S.; Ghosh, A. Graphene-MoS₂ Hybrid Structures for Multifunctional Photoresponsive Memory Devices. *Nat. Nanotechnol.* **2013**, *8* (11), 826–830.

(5) Yuan, H.; Liu, X.; Afshinmanesh, F.; Li, W.; Xu, G.; Sun, J.; Lian, B.; Curto, A. G.; Ye, G.; Hikita, Y.; Shen, Z.; Zhang, S.-C.; Chen, X.; Brongersma, M.; Hwang, H. Y.; Cui, Y. Polarization-Sensitive Broadband Photodetector Using a Black Phosphorus Vertical P-N Junction. *Nat. Nanotechnol.* **2015**, *10* (8), 707–713.

(6) Koppens, F. H.; Mueller, T.; Avouris, P.; Ferrari, A. C.; Vitiello, M. S.; Polini, M. Photodetectors Based on Graphene, Other Two-Dimensional Materials and Hybrid Systems. *Nat. Nanotechnol.* **2014**, *9* (10), 780–793.

(7) Xia, F.; Mueller, T.; Lin, Y.-m.; Valdes-Garcia, A.; Avouris, P. Ultrafast Graphene Photodetector. *Nat. Nanotechnol.* **2009**, *4* (12), 839–843.

(8) Choi, W.; Cho, M. Y.; Konar, A.; Lee, J. H.; Cha, G. B.; Hong, S. C.; Kim, S.; Kim, J.; Jena, D.; Joo, J.; Kim, S. High-Detectivity Multilayer MoS₂ Phototransistors with Spectral Response from Ultraviolet to Infrared. *Adv. Mater.* **2012**, *24* (43), 5832–5836.

(9) Island, J. O.; Blanter, S. I.; Buscema, M.; van der Zant, H. S.; Castellanos-Gomez, A. Gate Controlled Photocurrent Generation Mechanisms in High-Gain In₂Se₃ Phototransistors. *Nano Lett.* **2015**, *15* (12), 7853–7858.

(10) Mueller, T.; Xia, F.; Avouris, P. Graphene Photodetectors for High-Speed Optical Communications. *Nat. Photonics* **2010**, *4* (5), 297–301.

(11) Zhang, B. Y.; Liu, T.; Meng, B.; Li, X.; Liang, G.; Hu, X.; Wang, Q. J. Broadband High Photoresponse from Pure Monolayer Graphene Photodetector. *Nat. Commun.* **2013**, *4* (1), 1–11.

(12) Chhowalla, M.; Shin, H. S.; Eda, G.; Li, L.-J.; Loh, K. P.; Zhang, H. The Chemistry of Two-Dimensional Layered Transition Metal Dichalcogenide Nanosheets. *Nat. Chem.* **2013**, *5* (4), 263–275.

(13) Zhao, W.; Ghorannevis, Z.; Amara, K. K.; Pang, J. R.; Toh, M.; Zhang, X.; Kloc, C.; Tan, P. H.; Eda, G. Lattice Dynamics in Mono- and Few-Layer Sheets of WS₂ and WSe₂. *Nanoscale* **2013**, *5* (20), 9677–9683.

(14) Octon, T. J.; Nagareddy, V. K.; Russo, S.; Craciun, M. F.; Wright, C. D. Fast High-Responsivity Few-Layer MoTe₂ Photodetectors. *Adv. Opt. Mater.* **2016**, *4* (11), 1750–1754.

(15) Tu, L.; Cao, R.; Wang, X.; Chen, Y.; Wu, S.; Wang, F.; Wang, Z.; Shen, H.; Lin, T.; Zhou, P.; Meng, X.; Hu, W.; Liu, Q.; Wang, J.; Liu, M.; Chu, J. Ultrasensitive Negative Capacitance Phototransistors. *Nat. Commun.* **2020**, *11* (1), 101.

(16) Tao, L.; Cinquanta, E.; Chiappe, D.; Grazianetti, C.; Fanciulli, M.; Dubey, M.; Molle, A.; Akinwande, D. Silicene Field-Effect Transistors Operating at Room Temperature. *Nat. Nanotechnol.* **2015**, *10* (3), 227–231.

(17) Li, L.; Yu, Y.; Ye, G. J.; Ge, Q.; Ou, X.; Wu, H.; Feng, D.; Chen, X. H.; Zhang, Y. Black Phosphorus Field-Effect Transistors. *Nat. Nanotechnol.* **2014**, *9* (5), 372–377.

(18) Mudd, G. W.; Svatek, S. A.; Hague, L.; Makarovskiy, O.; Kudrynskiy, Z. R.; Mellor, C. J.; Beton, P. H.; Eaves, L.; Novoselov, K. S.; Kovalyuk, Z. D.; Vdovin, E. E.; Marsden, A. J.; Wilson, N. R.; Patane, A. High Broad-Band Photoresponsivity of Mechanically Formed InSe-Graphene Van Der Waals Heterostructures. *Adv. Mater.* **2015**, *27* (25), 3760–3766.

(19) Sucharitakul, S.; Goble, N. J.; Kumar, U. R.; Sankar, R.; Bogorad, Z. A.; Chou, F. C.; Chen, Y. T.; Gao, X. P. Intrinsic Electron Mobility Exceeding 10³ Cm²/(V S) in Multilayer InSe FETs. *Nano Lett.* **2015**, *15* (6), 3815–3819.

(20) Huang, W.; Gan, L.; Li, H.; Ma, Y.; Zhai, T. 2D Layered Group IIIA Metal Chalcogenides: Synthesis, Properties and Applications in Electronics and Optoelectronics. *CrystEngComm* **2016**, *18* (22), 3968–3984.

(21) Wu, F.; Xia, H.; Sun, H.; Zhang, J.; Gong, F.; Wang, Z.; Chen, L.; Wang, P.; Long, M.; Wu, X.; Wang, J.; Ren, W.; Chen, X.; Lu, W.;

Hu, W. AsP/InSe Van Der Waals Tunneling Heterojunctions with Ultrahigh Reverse Rectification Ratio and High Photosensitivity. *Adv. Funct. Mater.* **2019**, *29* (12), 1900314.

(22) Shang, H.; Chen, H.; Dai, M.; Hu, Y.; Gao, F.; Yang, H.; Xu, B.; Zhang, S.; Tan, B.; Zhang, X.; Hu, P. A Mixed-Dimensional 1D Se-2D InSe Van Der Waals Heterojunction for High Responsivity Self-Powered Photodetectors. *Nanoscale Horiz.* **2020**, *5* (3), 564–572.

(23) Feng, W.; Zheng, W.; Cao, W.; Hu, P. Back Gated Multilayer InSe Transistors with Enhanced Carrier Mobilities Via the Suppression of Carrier Scattering from a Dielectric Interface. *Adv. Mater.* **2014**, *26* (38), 6587–6593.

(24) Lei, S.; Ge, L.; Najmaei, S.; George, A.; Kappera, R.; Lou, J.; Chhowalla, M.; Yamaguchi, H.; Gupta, G.; Vajtai, R.; Mohite, A. D.; Ajayan, P. M. Evolution of the Electronic Band Structure and Efficient Photo-Detection in Atomic Layers of InSe. *ACS Nano* **2014**, *8* (2), 1263–1272.

(25) Tamalampudi, S. R.; Lu, Y. Y.; Kumar, U. R.; Sankar, R.; Liao, C. D.; Moorthy, B. K.; Cheng, C. H.; Chou, F. C.; Chen, Y. T. High Performance and Bendable Few-Layered InSe Photodetectors with Broad Spectral Response. *Nano Lett.* **2014**, *14* (5), 2800–2806.

(26) Yang, Z.; Jie, W.; Mak, C. H.; Lin, S.; Lin, H.; Yang, X.; Yan, F.; Lau, S. P.; Hao, J. Wafer-Scale Synthesis of High-Quality Semiconducting Two-Dimensional Layered InSe with Broadband Photoresponse. *ACS Nano* **2017**, *11* (4), 4225–4236.

(27) Tao, L.; Li, Y. N-Channel and P-Channel Few-Layer InSe Photoelectric Devices. *RSC Adv.* **2017**, *7* (78), 49694–49700.

(28) Wang, Y.; Zhang, J.; Liang, G.; Shi, Y.; Zhang, Y.; Kudrynskiy, Z. R.; Kovalyuk, Z. D.; Patanè, A.; Xin, Q.; Song, A. Schottky-Barrier Thin-Film Transistors Based on HfO₂-Capped InSe. *Appl. Phys. Lett.* **2019**, *115* (3), 033502.

(29) Chang, P.; Liu, X.; Liu, F.; Du, G. Remote Phonon Scattering in Two-Dimensional InSe FETs with High-κ Gate Stack. *Micromachines* **2018**, *9* (12), 674.

(30) Wells, S. A.; Henning, A.; Gish, J. T.; Sangwan, V. K.; Lauhon, L. J.; Hersam, M. C. Suppressing Ambient Degradation of Exfoliated InSe Nanosheet Devices Via Seeded Atomic Layer Deposition Encapsulation. *Nano Lett.* **2018**, *18* (12), 7876–7882.

(31) Ho, P. H.; Chang, Y. R.; Chu, Y. C.; Li, M. K.; Tsai, C. A.; Wang, W. H.; Ho, C. H.; Chen, C. W.; Chiu, P. W. High-Mobility InSe Transistors: The Role of Surface Oxides. *ACS Nano* **2017**, *11* (7), 7362–7370.

(32) Tsai, T. H.; Yang, F. S.; Ho, P. H.; Liang, Z. Y.; Lien, C. H.; Ho, C. H.; Lin, Y. F.; Chiu, P. W. High-Mobility InSe Transistors: The Nature of Charge Transport. *ACS Appl. Mater. Interfaces* **2019**, *11* (39), 35969–35976.

(33) Morozovska, A. N.; Strikha, M. V. Pyroelectric Origin of the Carrier Density Modulation at Graphene-Ferroelectric Interface. *J. Appl. Phys.* **2013**, *114* (1), 014101.

(34) Zhang, X.; Huang, H.; Yao, X.; Li, Z.; Zhou, C.; Zhang, X.; Chen, P.; Fu, L.; Zhou, X.; Wang, J.; Hu, W.; Lu, W.; Zou, J.; Tan, H. H.; Jagadish, C. Ultrasensitive Mid-Wavelength Infrared Photo-detection Based on a Single InAs Nanowire. *ACS Nano* **2019**, *13* (3), 3492–3499.

(35) Wang, X.; Wang, P.; Wang, J.; Hu, W.; Zhou, X.; Guo, N.; Huang, H.; Sun, S.; Shen, H.; Lin, T.; Tang, M.; Liao, L.; Jiang, A.; Sun, J.; Meng, X.; Chen, X.; Lu, W.; Chu, J. Ultrasensitive and Broadband MoS₂ Photodetector Driven by Ferroelectrics. *Adv. Mater.* **2015**, *27* (42), 6575–6581.

(36) Huang, H.; Wang, X.; Wang, P.; Wu, G.; Chen, Y.; Meng, C.; Liao, L.; Wang, J.; Hu, W.; Shen, H.; Lin, T.; Sun, J.; Meng, X.; Chen, X.; Chu, J. Ferroelectric Polymer Tuned Two Dimensional Layered MoTe₂ Photodetector. *RSC Adv.* **2016**, *6* (90), 87416–87421.

(37) Wang, X.; Shen, H.; Chen, Y.; Wu, G.; Wang, P.; Xia, H.; Lin, T.; Zhou, P.; Hu, W.; Meng, X.; Chu, J.; Wang, J. Multimechanism Synergistic Photodetectors with Ultrabroad Spectrum Response from 375 nm to 10 μm. *Adv. Sci.* **2019**, *6* (15), 1901050.

(38) Wu, G.; Tian, B.; Liu, L.; Lv, W.; Wu, S.; Wang, X.; Chen, Y.; Li, J.; Wang, Z.; Wu, S.; Shen, H.; Lin, T.; Zhou, P.; Liu, Q.; Duan, C.; Zhang, S.; Meng, X.; Wu, S.; Hu, W.; Wang, X.; Chu, J.; Wang, J.

Programmable Transition Metal Dichalcogenide Homojunctions Controlled by Nonvolatile Ferroelectric Domains. *Nat. Electron.* **2020**, *3* (1), 43–50.

(39) De Blasi, C.; Micocci, G.; Mongelli, S.; Tepore, A. Large InSe Single Crystals Grown from Stoichiometric and Non-Stoichiometric Melts. *J. Cryst. Growth* **1982**, *57* (3), 482–486.

(40) Zeng, J.; Liang, S.-J.; Gao, A.; Wang, Y.; Pan, C.; Wu, C.; Liu, E.; Zhang, L.; Cao, T.; Liu, X.; Fu, Y.; Wang, Y.; Watanabe, K.; Taniguchi, T.; Lu, H.; Miao, F. Gate-Tunable Weak Antilocalization in a Few-Layer InSe. *Phys. Rev. B: Condens. Matter Mater. Phys.* **2018**, *98* (12), 125414.

(41) Zhao, D.; Lenz, T.; Gelinck, G. H.; Groen, P.; Damjanovic, D.; de Leeuw, D. M.; Katsouras, I. Depolarization of Multidomain Ferroelectric Materials. *Nat. Commun.* **2019**, *10* (1), 1–11.

(42) Radisavljevic, B.; Radenovic, A.; Brivio, J.; Giacometti, V.; Kis, A. Single-Layer MoS₂ Transistors. *Nat. Nanotechnol.* **2011**, *6* (3), 147–150.

(43) Gao, A.; Lai, J.; Wang, Y.; Zhu, Z.; Zeng, J.; Yu, G.; Wang, N.; Chen, W.; Cao, T.; Hu, W.; Sun, D.; Chen, X.; Miao, F.; Shi, Y.; Wang, X. Observation of Ballistic Avalanche Phenomena in Nanoscale Vertical InSe/BP Heterostructures. *Nat. Nanotechnol.* **2019**, *14* (3), 217–222.

(44) Wu, L.; Shi, J.; Zhou, Z.; Yan, J.; Wang, A.; Bian, C.; Ma, J.; Ma, R.; Liu, H.; Chen, J.; Huang, Y.; Zhou, W.; Bao, L.; Ouyang, M.; Pantelides, S. T.; Gao, H.-J. InSe/hBN/Graphite Heterostructure for High-Performance 2D Electronics and Flexible Electronics. *Nano Res.* **2020**, *13* (4), 1127–1132.

(45) Wang, X.; Chen, Y.; Wu, G.; Wang, J.; Tian, B.; Sun, S.; Shen, H.; Lin, T.; Hu, W.; Kang, T.; Tang, M.; Xiao, Y.; Sun, J.; Meng, X.; Chu, J. Graphene Dirac Point Tuned by Ferroelectric Polarization Field. *Nanotechnology* **2018**, *29* (13), 134002.

(46) Zheng, D.; Wang, J.; Hu, W.; Liao, L.; Fang, H.; Guo, N.; Wang, P.; Gong, F.; Wang, X.; Fan, Z.; Wu, X.; Meng, X.; Chen, X.; Lu, W. When Nanowires Meet Ultrahigh Ferroelectric Field-High-Performance Full-Depleted Nanowire Photodetectors. *Nano Lett.* **2016**, *16* (4), 2548–55.

(47) Yin, C.; Wang, X.; Chen, Y.; Li, D.; Lin, T.; Sun, S.; Shen, H.; Du, P.; Sun, J.; Meng, X.; Chu, J.; Wong, H. F.; Leung, C. W.; Wang, Z.; Wang, J. A Ferroelectric Relaxor Polymer-Enhanced P-Type WSe₂ Transistor. *Nanoscale* **2018**, *10* (4), 1727–1734.

(48) Zhang, W.; Huang, J. K.; Chen, C. H.; Chang, Y. H.; Cheng, Y. J.; Li, L. J. High-Gain Phototransistors Based on a CVD MoS₂ Monolayer. *Adv. Mater.* **2013**, *25* (25), 3456–3461.

(49) Konstantatos, G.; Sargent, E. H. Nanostructured Materials for Photon Detection. *Nat. Nanotechnol.* **2010**, *5* (6), 391–400.

(50) Yang, T.; Zheng, B.; Wang, Z.; Xu, T.; Pan, C.; Zou, J.; Zhang, X.; Qi, Z.; Liu, H.; Feng, Y.; Hu, W.; Miao, F.; Sun, L.; Duan, X.; Pan, A. Van Der Waals Epitaxial Growth and Optoelectronics of Large-Scale WSe₂/SnS₂ Vertical Bilayer P-N Junctions. *Nat. Commun.* **2017**, *8* (1), 1–9.

(51) Feng, W.; Zheng, W.; Chen, X.; Liu, G.; Hu, P. Gate Modulation of Threshold Voltage Instability in Multilayer InSe Field Effect Transistors. *ACS Appl. Mater. Interfaces* **2015**, *7* (48), 26691–26695.

(52) Liu, Y.; Weiss, N. O.; Duan, X.; Cheng, H.-C.; Huang, Y.; Duan, X. Van Der Waals Heterostructures and Devices. *Nat. Rev. Mater.* **2016**, *1* (9), 1–17.

(53) Castellanos-Gomez, A.; Buscema, M.; Molenaar, R.; Singh, V.; Janssen, L.; van der Zant, H. S. J.; Steele, G. A. Deterministic Transfer of Two-Dimensional Materials by All-Dry Viscoelastic Stamping. *2D Mater.* **2014**, *1* (1), 011002.